

Fig. 1. Schematic of the DAMPE instrument.

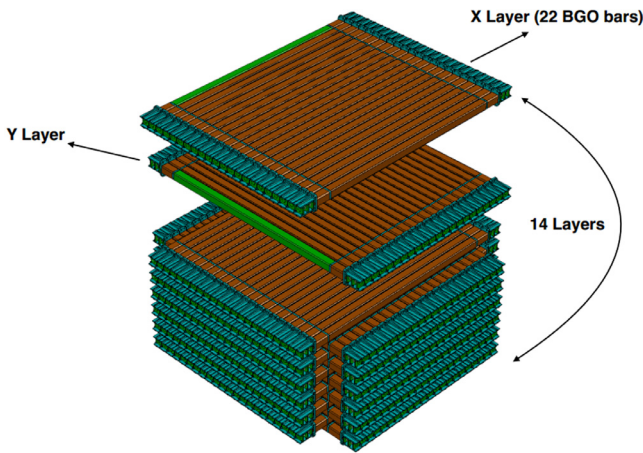


Fig. 2. Structure of the BGO electromagnetic calorimeter.

are coupled at the ends of each crystal bar to collect fluorescence. Two PMTs and a BGO crystal bar form a sensitive unit (SU), resulting in a total of 308 SUs. The whole calorimeter has a good energy resolution of 1.5% at 800 GeV for high-energy cosmic-ray electrons/positrons and γ -rays, and covers a wide energy range of 5 GeV–10 TeV [1,15–17].

The calibration of an individual SU requires the determination of the conversion coefficient between the signal output in digital counts (ADC) from the electronics and the energy deposited in the crystal. The conversion coefficients are defined as follows:

$$k_{(i,j)} \equiv \frac{E_{(i,j)}}{ADC_{(i,j)}} \quad (1)$$

where $E_{(i,j)}$ is the absolute energy deposition measured by the j_{th} PMT of the i_{th} BGO crystal bar, $ADC_{(i,j)}$ is the corresponding ADC output of that channel in orbit data, and $k_{(i,j)}$ is the conversion coefficient. The $k_{(i,j)}$ value varies between individual SUs depending on many aspects of the SU performance, such as, the light yield of the crystal, the PMT gain, and the attenuation coefficient of the filter coupled between the crystal and the PMT [1]. On the ground, cosmic-ray muons and test beams [15,18] have been used to obtain these conversion coefficients. However, during the in-orbit phase, the absence of muon or other mono-energetic source for calibration is a crucial issue.

Herein, we introduce the approach in the DAMPE experiment. Firstly, a reference energy $E_{(i,j)}$ should be determined. Approximately 20% of cosmic-ray protons pass through the whole BGO calorimeter only with ionization energy loss, whereas the majority of them interact with the calorimeter material forming a hadronic shower. Those

penetration events, whose $\beta\gamma$ does not exactly fall in the minimum ionizing particle (MIP) region, are defined as quasi Minimum Ionizing Particles (q-MIPs) because their behavior is similar to those of MIPs. The peak position of the q-MIPs' ionization energy loss spectrum can be predicted via simulation and are therefore taken as an energy reference $E_{(i,j)}$. Secondly, we select the q-MIPs in orbit data and yield their ADC spectrum. Then, conversion coefficients can be derived by comparison of the peak positions between the simulated energy spectrum and the ADC spectrum. In a real calibration process, more details should be considered. These will be discussed in the following sections.

2.1. Orbit simulation

Generally, cosmic ray protons' flux follows a power law distribution with an index of -2.7 . However, in the low energy range (<10 GeV), the flux is influenced by many aspects, including the geomagnetic field of the Earth, which shields the low energy cosmic rays, and the solar activities, which affects shape of the flux spectrum. Secondary protons, which are produced in the interaction between primary particles and the atmosphere, also contribute to the spectrum. The flux represents the kinetic energy distribution of q-MIPs, and will finally influence the peak position of the ionization loss spectrum for each SU. Thus, an orbit simulation is conducted to describe the proton flux accurately.

ATmospheric Muon Neutrino Calculation 3-dimensional version (ATMNC3) package [19,20], which is a simulation code originally developed for the calculation of atmospheric muons and neutrinos, is adopted to generate the proton flux. ATMNC3 can simulate charged particles traveling in the Earth's geomagnetic field at a given time, and importantly, it can also well describe the flux component contributed by secondary protons. In the package, we adopted the International Geomagnetic Reference Field (IGRF) 2015 [21] for the geomagnetic field description, and set the altitude to 500 km, which is the average altitude of the real DAMPE orbit.

Fig. 3 shows the ATMNC3-generated spatial distribution of protons with energy higher than 0.1 GeV at an altitude of 500 km. The South Atlantic Anomaly (SAA) area, which is located at approximately -20° latitude and -70° longitude, is clearly visible in the picture. The data in this region are rejected in the offline analysis.

Fig. 4 shows the simulated proton fluxes at different geomagnetic latitudes. Cutoffs caused by geomagnetic rigidity can be clearly observed in the spectra, especially at lower geomagnetic latitudes (smaller Θ_M in the figure). The cutoff values decrease as the geomagnetic latitude increases because the intensity of the magnetic field weakens when the satellite approaches the poles. Usually, events with energy larger than the cutoff are classified as primary particles, whereas the ones with energy below the cutoff are classified as secondary particles. The AMS-01 experimental data [22] are also plotted in the figure for comparison. The agreement between the shape of the cutoff in the simulation and the AMS-01 results worsens as the geomagnetic latitude increases. This is due to the fact that solar activities might not be described well in the ATMNC3 package. Nevertheless, the simulated flux at a low geomagnetic latitude is still reliable because solar activities mainly have greater influence on low-energy protons at high geomagnetic latitudes.

The proton flux spectrum around the orbit of the DAMPE, generated by the ATMNC3 package, is then taken as the input for use in GEANT4 (version 10.02.p01) to simulate interaction between the particles and the DAMPE detector. Also noteworthy is the fact that, calibration parameters extracted from orbit data are applied in the GEANT4 simulation to digitize the simulated detector response properly. These parameters rely on a precise SU calibration. Thus, the simulation and subsequent calibration procedures are iterated several times until stable parameters are derived. Simulation data are saved with the same format as that of the real data so that the same reconstruction and analysis algorithms can be used to process the two data-sets.

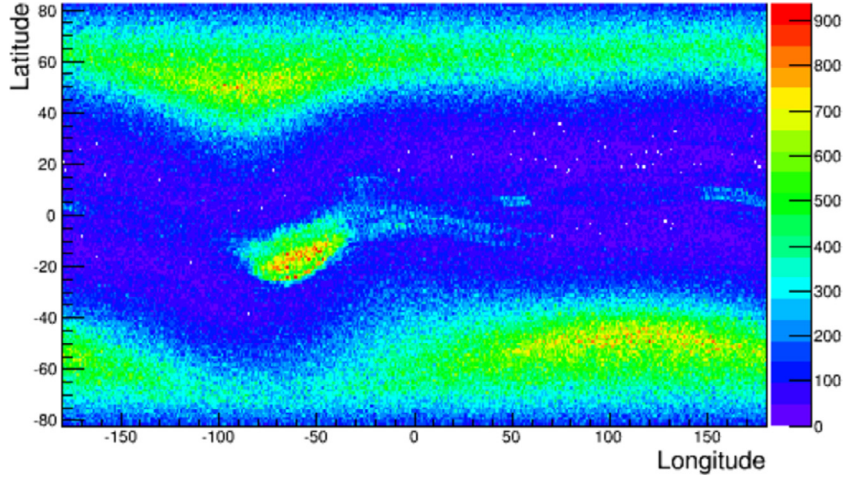


Fig. 3. Spatial distribution of protons ($>0.1\text{GeV}$) produced by ATMNC3 for altitude of 500 km.

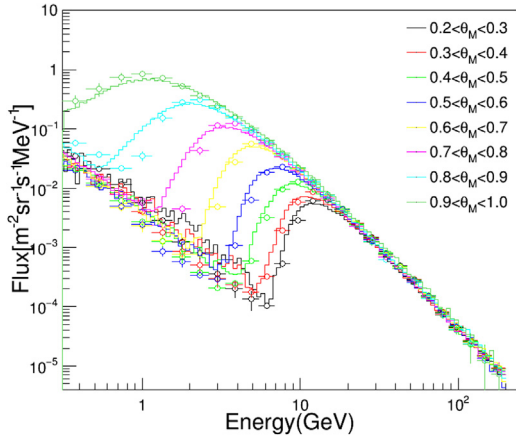


Fig. 4. Proton flux spectra generated by ATMNC3 at different geomagnetic latitudes (θ_M), compared to results observed by AMS-01 at an altitude of 400 km. Hollow points denote results for AMS-01 [22], whereas solid lines denote results for ATMNC3.

2.2. Selection of q -MIPs

The DAMPE detector has five trigger logics. One of them, called the MIPs trigger, is specifically designed for q -MIP events [23]. Considering the good agreement of ATMNC3 simulation at a low latitude near the equator, it is only turned on when the satellite is between latitudes -20° and $+20^\circ$ in space. In order to select q -MIPs, a series of selection criteria are applied as follows:

1. MIPs trigger selection: Reject the particles that do not satisfy the MIPs trigger and those beyond the $\pm 20^\circ$ latitudes.
2. Global track selection: Reject the particles that fail to be reconstructed as good quality tracks in the detectors.
3. Charge selection: Only single-charged events are retained.
4. Energy selection: This is a somewhat loose criterion to reject the events apparently creating shower. It simply requires that the energy deposition in the calorimeter should be lower than 40 times the MIP energy deposit in a single bar (approximately 1200 MeV).
5. Number of hits in a layer selection: Reject particles with more than two hits in any layer of the BGO calorimeter.
6. Likelihood selection: Reject the particles with a likelihood function value located outside the proton q -MIPs distribution. This likelihood function value is calculated as the logarithm value of the scalar product of likelihood function values for 14 layers.

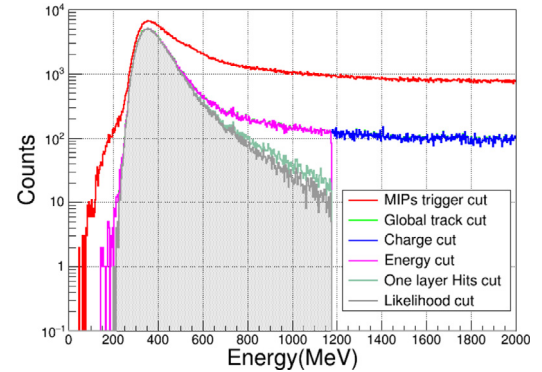


Fig. 5. Spectra of the ionization energy loss in the BGO calorimeter after the application of the proton MIP selection criteria. The gray shaded area represents proton q -MIP candidates.

Based on the aforementioned six criteria, the proton q -MIPs candidates from both Monte Carlo (MC) simulation data and experimental data are obtained. Fig. 5 shows how the distribution of the total energy deposition of the MC simulation protons in the BGO calorimeter varies with respect to the six criteria. The events in the gray shaded region around 320 MeV are selected as the MC simulation samples of the proton q -MIP candidates.

2.3. Determination of the conversion coefficients of SUs

After the selection of q -MIPs, an ionization energy loss spectrum for simulated proton q -MIPs and an ADC spectrum for orbit data are derived. Fig. 6 shows a typical spectrum of the energy deposition of the SU of Bar#12/L#01 (bar 12 in layer 1), and a Landau function convoluted by a Gaussian function is used to fit the spectrum, where the fitting parameters p_0 , p_1 , p_2 , and p_3 represent the Landau width, MPV, area, and Gaussian width, respectively. The peak value of the fitting function is regarded as the energy reference ($E_{(i,j)}$ in Eq. (1)) for this SU.

For the orbit data, the q -MIP proton candidates are obtained using the same selection criteria as that applied in simulation. The ADC signal spectrum of q -MIP protons is expected to exhibit the same shape as the orbit. Fig. 7 shows a typical ADC signal spectrum of the SU of Bar#12/L#01. The $ADC_{(i,j)}$ in Eq. (1) for the SU is defined as the peak value of the fitting function of the ADC spectrum.

Using this method, a total of 616 conversion coefficients $k_{(i,j)}$ for all 308 SUs are properly calibrated.

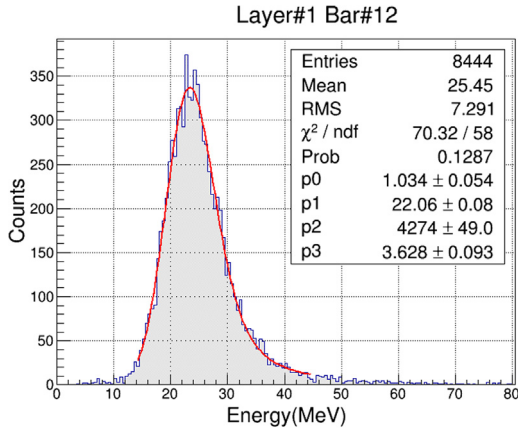


Fig. 6. Ionization energy loss spectrum of simulated q-MIP protons from SU of Bar#12/L#01. Red line is fit using a Landau function convoluted with an Gaussian function.

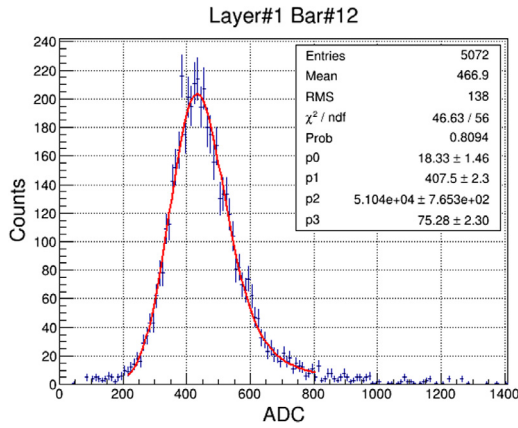


Fig. 7. Ionization energy loss spectrum (ADC) of experimental q-MIP protons from SU of Bar#12/L#01. Red line is fit using a Landau function convoluted with an Gaussian function.

3. Performance of sensitive unit calibration

3.1. Performance of conversion coefficients

During the whole operating time, the conversion coefficients $k_{(i,j)}$ are not invariable. Temperature variation in space mainly affects the light yield of BGO crystals, and then affects the values of $ADC_{(i,j)}$ s and $k_{(i,j)}$ s [10,24]. Fig. 8 shows one channel's daily $ADC_{(i,j)}$ changing with temperature in nearly 5.5 years. Concerning the temperature changes slowly (approximately 0.1%/day), any short-term temperature effect could be negligible. Therefore, to correct such effects, the SU calibration is conducted daily, and the corresponding conversion coefficients are applied to reconstruct data of each day. We have also studied the energy measurement performance over the long term. The reconstructed energy stability of proton q-MIPs is better than 1% subsequent to temperature correction. Details can be found in [2,9].

Other calorimeter performance parameters, including pedestal noises, PMT gains, and attenuation lengths of long BGO crystals, are also extensively calibrated with the orbit data [2,25], and applied in the energy reconstruction. The full reconstruction procedure has been reported in [1].

3.2. Precision of sensitive unit calibration

To estimate the precision of SU calibration, a helium data set is examined. A similar approach is adopted to generate the ATMNC3

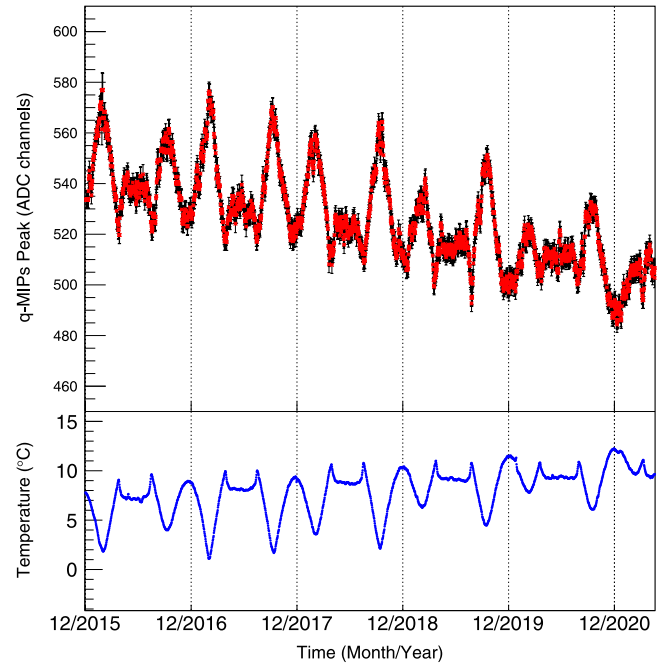


Fig. 8. Variations of one channel's $ADC_{(i,j)}$ value (upper panel) and its temperature (lower panel) with time.

helium flux, simulate the detector response, select q-MIPs, and yield ionization energy loss spectrum. In contrast to protons, secondary helium is rarely produced in atmosphere, which is also considered in ATMNC3 simulation. The helium q-MIPs spectra, derived from both orbit data and simulation, are compared in Fig. 9(b). Meanwhile, as a self assessment of the SU calibration, the proton q-MIP spectrum is compared with the simulated one in Fig. 9(a).

A Landau function convoluted with a Gaussian function is used to fit the spectra of proton and helium q-MIPs. Peak values of the function fitting the proton spectra are 321.3 ± 0.1 MeV for orbit simulation and 322.3 ± 0.1 MeV for flight data. The results of helium spectra are 1294.1 ± 1.1 MeV and 1305 ± 2.0 MeV for orbit simulation and flight data, respectively. The deviation between the helium spectra obtained by simulation and flight data, which is lower than 1%, is taken as the precision of the SU calibration.

3.3. Verification with proton q-MIPs at different geomagnetic latitudes

The effect of the geomagnetic field on the distribution of an orbit proton flux has been shown in Fig. 4. This effect can be used to verify the accuracy of the orbit simulation based on the ATMNC3 software. Shortly after the satellite was launched, DAMPE spent three days taking data using the MIPs trigger at all the orbit latitudes. These data samples were used to assess the response of the BGO calorimeter to the ionization energy loss of q-MIP events at different geomagnetic latitudes. The orbit simulations of the protons at different geomagnetic latitudes are implemented. Fig. 10 shows the peaks of the proton q-MIP's energy spectra as a function of the geomagnetic latitude. The deviation between the simulation result and the flight data at a relatively low geomagnetic latitude, whereas it is less than 1%, increases to 4% at high latitudes. This could be contributed to the imperfect description of solar activities in ATMNC3, as discussed above.

3.4. Verification with geomagnetic cutoff measurement

To further verify the energy reconstruction, we measure the geomagnetic cutoff of cosmic rays with the energy depositions of their

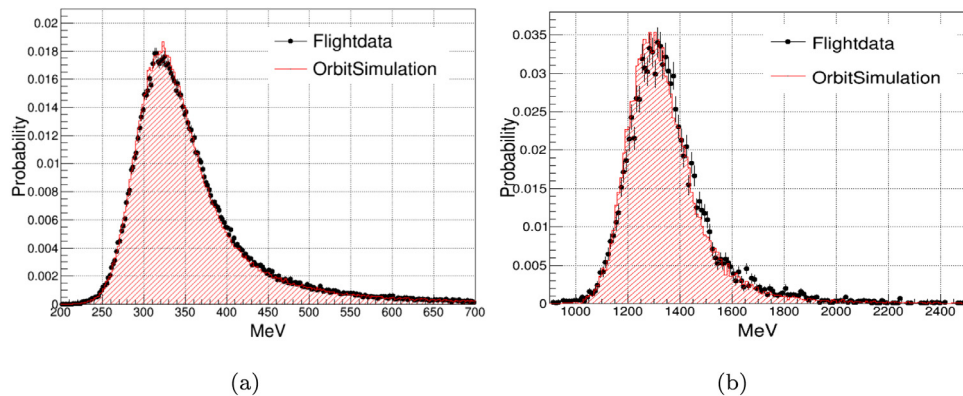


Fig. 9. Spectra of ionization energy loss of proton q-MIPs (a) and helium q-MIPs (b). Histogram is orbit simulation results, and black point is experimental (flight) results.

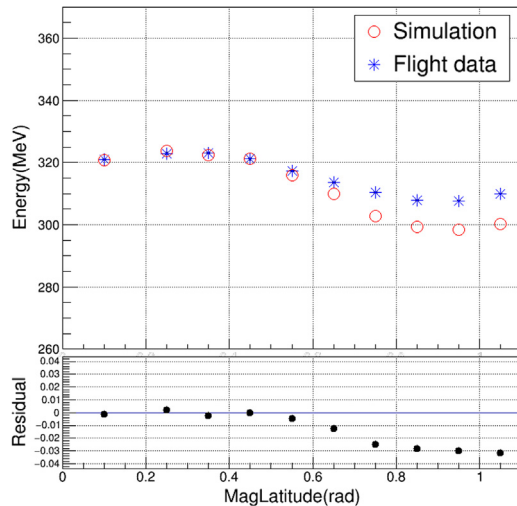


Fig. 10. Ionization energy loss of q-MIP protons in BGO calorimeter at different geomagnetic latitude ranges. Blue stars represent the flight data, and red circles represent orbit simulation. The bottom panel visualizes the residual of flight data and orbit simulation, where residual is defined as (simulated energy - experimental energy) / simulated energy.

showered particles. A preliminary result of measuring electron's geomagnetic cutoff shows approximately 1% deviation of energy scale at 13 GeV [26], which is treated as the energy measurement uncertainty. A formal study about this issue is currently under preparation. The cutoff measurement of cosmic-ray nuclei, although the calorimeter's energy resolution for nuclei is much worse than that for electrons, has also been discussed in [27].

4. Conclusion

We have developed a reasonable and appropriate method for the in-orbit calibration of DAMPE calorimeter SUs. Ionization energy loss when cosmic ray proton q-MIPs pass through a BGO crystal is taken as the energy reference, and the conversion coefficients between the electronics output in digital counts and the real energy deposition are then determined. Several approaches are performed to verify the calibration performance, such as validation with proton and helium q-MIPs, measuring the geomagnetic cutoff of cosmic rays, and studying the long term performance of energy reconstruction. These results show that a stable and homogeneous inter-calibration for the DAMPE calorimeter has been achieved. The proposed method provides a reliable basis for subsequent physical analysis.

CRediT authorship contribution statement

S.C. Wen: Formal analysis, Data curation, Investigation, Writing – original draft. **Y.F. Wei:** Writing – review & editing, Validation, Funding acquisition. **Z.Y. Zhang:** Conceptualization, Funding acquisition. **Y.L. Zhang:** Conceptualization, Supervision, Funding acquisition. **L.B. Wu:** Validation. **H.T. Dai:** Validation. **C.M. Liu:** Validation. **C. Zhao:** Validation. **Y. Wang:** Validation. **X.L. Wang:** Conceptualization. **Z.Z. Xu:** Conceptualization. **G.S. Huang:** Supervision, Funding acquisition. **W. Jiang:** Software. **Y.Q. Zhang:** Validation. **P.X. Ma:** Validation. **W.H. Li:** Validation. **C. Yue:** Validation, Data curation. **P. Fusco:** Validation. **E. Casilli:** Validation. **A. Parenti:** Validation. **L. Silveri:** Validation. **E. Catanzani:** Validation.

Declaration of competing interest

The authors declare that they have no known competing financial interests or personal relationships that could have appeared to influence the work reported in this paper.

Acknowledgments

This work is supported by the Outstanding Youth Science Foundation of NSFC (Grant No. 12022503), the Joint Funds of the National Natural Science Foundation of China (Grant No. U1738208, U1738139 and U1738135), the National Natural Science Foundation of China (Grant No. 11673021, 11705197 and 11851302), the National Key Research and Development Program of China (Grant No. 2016YFA0400200), the Youth Innovation Promotion Association CAS (Grant No. 2021450), and the Natural Science Foundation of Jiangsu Province, China (Grant No. BK20201107).

References

- [1] J. Chang, G. Ambrosi, Q. An, R. Asfandiyarov, P. Azzarello, P. Bernardini, B. Bertucci, M. Cai, M. Caragiulo, D. Chen, et al., The Dark Matter Particle Explorer mission, Astropart. Phys. 95 (2017) 6–24.
- [2] G. Ambrosi, Q. An, R. Asfandiyarov, P. Azzarello, P. Bernardini, M. Cai, M. Caragiulo, J. Chang, D. Chen, H. Chen, et al., The on-orbit calibration of Dark Matter Particle Explorer, Astropart. Phys. 106 (2019) 18–34.
- [3] Y. Yu, Z. Sun, H. Su, Y. Yang, J. Liu, J. Kong, G. Xiao, X. Ma, Y. Zhou, H. Zhao, et al., The plastic scintillator detector for DAMPE, Astropart. Phys. 94 (2017) 1–10.
- [4] P. Azzarello, G. Ambrosi, R. Asfandiyarov, P. Bernardini, B. Bertucci, A. Bolognini, F. Cadoux, M. Caprai, I. De Mitri, M. Domenzoz, et al., The DAMPE silicon-tungsten tracker, Nucl. Instrument. Methods Phys. Res. Sect. A: Accel. Spectromet. Detect. Associat. Equip. 831 (2016) 378–384.
- [5] Z. Zhang, Y. Zhang, J. Dong, S. Wen, C. Feng, C. Wang, Y. Wei, X. Wang, Z. Xu, S. Liu, Design of a high dynamic range photomultiplier base board for the BGO ECAL of DAMPE, Nucl. Instrument. Methods Phys. Res. Sect. A: Accel. Spectromet. Detect. Associat. Equip. 780 (2015) 21–26.

- [6] H. Ming, M. Tao, C. Jin, Z. Yan, H. Yong-yi, Z. Jing-jing, W. Jian, D. Tie-kuang, GEANT4 simulation of neutron detector for DAMPE, Chin. Astronomy Astrophys. 40 (4) (2016) 474–482.
- [7] T. Dong, Y. Zhang, P. Ma, Y. Zhang, P. Bernardini, M. Ding, D. Guo, S. Lei, X. Li, I. De Mitri, et al., Charge measurement of cosmic ray nuclei with the plastic scintillator detector of DAMPE, Astropart. Phys. 105 (2019) 31–36.
- [8] A. Tykhonov, G. Ambrosi, R. Asfandiyarov, P. Azzarello, P. Bernardini, B. Bertucci, A. Bolognini, F. Cadoux, A. D'Amone, A. De Benedittis, et al., In-flight performance of the DAMPE silicon tracker, Nucl. Instrument. Methods Phys. Res. Sect. A: Accel. Spectromet. Detectors Associat. Equip. 924 (2019) 309–315.
- [9] L. Wu, S. Wen, C. Liu, H. Dai, Y. Wei, Z. Zhang, X. Wang, Z. Xu, C. Feng, S. Liu, et al., Calibration and status of the 3-D imaging calorimeter of DAMPE for cosmic ray physics on orbit, IEEE Trans. Nucl. Sci. 65 (8) (2018) 2007–2012.
- [10] Y.-P. Wang, S.-C. Wen, W. Jiang, C. Yue, Z.-Y. Zhang, Y.-F. Wei, Y. Zhang, J.-J. Zang, J. Wu, Temperature effects on MIPs in the BGO calorimeters of DAMPE, Chin. Phys. C 41 (10) (2017) 106001.
- [11] H. Zhao, W.-X. Peng, H.-Y. Wang, R. Qiao, D.-Y. Guo, H. Xiao, Z.-M. Wang, A machine learning method to separate cosmic ray electrons from protons from 10 to 100 GeV using DAMPE data, Res. Astronomy Astrophys. 18 (6) (2018) 071.
- [12] G. Ambrosi, Q. An, R. Asfandiyarov, P. Azzarello, P. Bernardini, B. Bertucci, M. Cai, J. Chang, D. Chen, H. Chen, et al., Direct detection of a break in the teraelectronvolt cosmic-ray spectrum of electrons and positrons, Nature 552 (7683) (2017) 63–66.
- [13] Q. An, R. Asfandiyarov, P. Azzarello, P. Bernardini, X. Bi, M. Cai, J. Chang, D. Chen, H. Chen, J. Chen, et al., Measurement of the cosmic ray proton spectrum from 40 GeV to 100 tev with the DAMPE satellite, Sci. Adv. 5 (9) (2019) eaax3793.
- [14] F. Alemanno, Q. An, P. Azzarello, F. Barbato, P. Bernardini, X. Bi, M. Cai, E. Catanzani, J. Chang, D. Chen, et al., Measurement of the cosmic ray helium energy spectrum from 70 GeV to 80 TeV with the DAMPE space mission, Phys. Rev. Lett. 126 (20) (2021) 201102.
- [15] Z. Zhang, C. Wang, J. Dong, Y. Wei, S. Wen, Y. Zhang, Z. Li, C. Feng, S. Gao, Z. Shen, et al., The calibration and electron energy reconstruction of the BGO ECAL of the DAMPE detector, Nucl. Instrument. Methods Phys. Res. Sect. A: Accel. Spectromet. Detect. Associat. Equip. 836 (2016) 98–104.
- [16] Z.-Y. Li, Z.-Y. Zhang, Y.-F. Wei, C. Wang, Y.-L. Zhang, S.-C. Wen, X.-L. Wang, Z.-Z. Xu, G.-S. Huang, Energy correction for the BGO calorimeter of DAMPE using an electron beam, Chin. Phys. C 40 (8) (2016) 086202.
- [17] C. Yue, J. Zang, T. Dong, X. Li, Z. Zhang, S. Zimmer, W. Jiang, Y. Zhang, D. Wei, A parameterized energy correction method for electromagnetic showers in BGO-ECAL of DAMPE, Nucl. Instrument. Methods Phys. Res. Sect. A: Accel. Spectromet. Detectors Associat. Equip. 856 (2017) 11–16.
- [18] Y. Wei, Y. Zhang, Z. Zhang, L. Wu, S. Wen, H. Dai, C. Liu, X. Wang, Z. Xu, G. Huang, et al., Performance of the DAMPE BGO calorimeter on the ion beam test, Nucl. Instrument. Methods Phys. Res. Sect. A: Accel. Spectromet. Detectors Associat. Equip. 922 (2019) 177–184.
- [19] M. Honda, T. Kajita, K. Kasahara, S. Midorikawa, New calculation of the atmospheric neutrino flux in a three-dimensional scheme, Phys. Rev. D 70 (4) (2004) 043008.
- [20] T. Niita, S. Torii, Y. Akaike, Y. Asaoka, K. Kasahara, S. Ozawa, T. Tamura, Energy calibration of calorimetric electron telescope (CALET) in space, Adv. Space Res. 55 (11) (2015) 2500–2508.
- [21] E. Thébault, C.C. Finlay, C.D. Beggan, P. Alken, J. Aubert, O. Barrois, F. Bertrand, T. Bondar, A. Boness, L. Brocco, et al., International geomagnetic reference field: the 12th generation, Earth Planets Space 67 (1) (2015) 1–19.
- [22] J. Alcaraz, D. Alvisi, B. Alpat, G. Ambrosi, H. Anderhub, L. Ao, A. Arefiev, P. Azzarello, E. Babucci, L. Baldini, et al., Protons in near earth orbit, Phys. Lett. B 472 (1–2) (2000) 215–226.
- [23] Y.-Q. Zhang, J.-H. Guo, Y. Liu, C.-Q. Feng, Y.-L. Zhang, T.-K. Dong, J.-J. Zang, C. Yue, Design and on-orbit status of the trigger system for the DAMPE mission, Res. Astronomy Astrophys. 19 (9) (2019) 123.
- [24] Y. Wei, Z.-Y. Zhang, Y. Zhang, S. Wen, C. Wang, Z. Li, C. Feng, X. Wang, Z. Xu, G. Huang, et al., Temperature dependence calibration and correction of the DAMPE BGO electromagnetic calorimeter, J. Instrument. 11 (07) (2016) T07003.
- [25] L.-B. Wu, Y.-L. Zhang, Z.-Y. Zhang, Y.-F. Wei, S.-C. Wen, H.-T. Dai, C.-M. Liu, X.-L. Wang, Z.-Z. Xu, G.-S. Huang, Energy correction based on fluorescence attenuation of DAMPE, Res. Astronomy Astrophys. 20 (8) (2020) 118.
- [26] J. Zang, C. Yue, X. Li, Measurement of absolute energy scale of ECAL of DAMPE with geomagnetic rigidity cutoff, in: Proc. Sci.(ICRC2017), vol. 197, 2017.
- [27] H. Dai, Y. Zhang, J. Zang, Z. Zhang, Y. Wei, L. Wu, C. Liu, C. Luo, D. Kyratzis, A. De Benedittis, et al., Response of the BGO calorimeter to cosmic-ray nuclei in the DAMPE experiment on orbit, IEEE Trans. Nucl. Sci. 67 (6) (2020) 956–961.